

1 **The endoplasmic reticulum-resident protein TMEM-120/TMEM120A promotes fat**
2 **storage in *C. elegans* and mammalian cells**

3

4 Yan Li¹, Siwei Huang¹, Xuesong Li², Xingyu Yang¹, Ningyi Xu³, Jianan Qu², Ho Yi Mak^{1,*}

5

6 1. Division of Life Science, The Hong Kong University of Science and Technology, Hong
7 Kong SAR, China.

8 2. Biophotonics Research Laboratory, Department of Electronic and Computer Engineering,
9 The Hong Kong University of Science and Technology, Hong Kong SAR, China.

10 3. The MOE Key Laboratory of Biosystems Homeostasis & Protection and Innovation Center
11 for Cell Signaling Network, Life Sciences Institute, Zhejiang University, Hangzhou,
12 Zhejiang, China.

13

14

15 * Corresponding author: hym@ust.hk ORCID: 0000-0002-1500-5328

16

17 **Keywords:** TMEM-120, TMEM120A, endoplasmic reticulum, lipid droplets

18 **Abstract**

19 The synthesis of triacylglycerol (TAG) is essential for the storage of excess fatty acids, which
20 can subsequently be used for energy or cell growth. A series of enzymes act in the
21 endoplasmic reticulum (ER) to synthesize TAG, prior to its transfer to lipid droplets (LDs),
22 which are conserved organelles for fat storage. Here, we report that the deficiency of TMEM-
23 120/TMEM120A, a protein with 6-transmembrane helices, retards TAG synthesis and LD
24 expansion in *C. elegans*. GFP fusion proteins of TMEM-120, expressed at the endogenous
25 level in live worms, were observed throughout the ER network. Using Stimulated Raman
26 Scattering, we demonstrated the specific requirement of TMEM-120 in the storage of
27 exogenous fatty acids in LDs. Knockdown of TMEM120A impedes adipogenesis of pre-
28 adipocytes in vitro, while its over-expression is sufficient to promote LD expansion in
29 mammalian cells. Our results suggest that TMEM-120/TMEM120A plays a conserved role in
30 increasing the efficiency of TAG synthesis.

31 **Introduction**

32 Excess fatty acids from de novo lipogenesis or the diet can be incorporated into
33 neutral fat, such as triacylglycerol (TAG), via the glycerol-3-phosphate (G3P) or the
34 monoacylglycerol (MAG) pathway (Yen et al., 2008). Common to both pathways is the
35 addition of fatty acyl-Coenzyme-A (acyl-CoA) molecules to specific positions of the glycerol
36 backbone, by acyltransferases (Coleman and Lee, 2004). Based on biochemical and imaging
37 analyses, all TAG biosynthetic enzymes can be found in the endoplasmic reticulum (ER).
38 Accordingly, newly synthesized TAG accumulates between ER membrane leaflets before the
39 directional budding of the cytoplasmic leaflet to form nascent lipid droplets (LDs), which are
40 conserved organelles for fat storage (Henne et al., 2018; Thiam and Ikonen, 2021; Walther et
41 al., 2017). Additional TAG synthesis occurs at ER-LD contacts to support LD expansion
42 (Cao and Mak, 2020; Olzmann and Carvalho, 2019; Schuldiner and Bohnert, 2017).
43 Although the core ensemble of TAG biosynthetic enzymes have been well-defined, it is
44 unknown if additional proteins are required for the maximal efficiency of TAG synthesis.

45 TMEM120A (alternatively known as NET29 or TACAN) is a member of a conserved
46 family of transmembrane proteins that had been assigned seemingly unrelated functions. It
47 was first reported in a proteomic study of the nuclear envelop (Schirmer et al., 2003).
48 Subsequent functional analysis indicates that TMEM120A, and its paralog TMEM120B, is
49 required for the differentiation of 3T3-L1 pre-adipocytes into mature adipocytes (Batrakou et
50 al., 2015). More recently, TMEM120A was reported to act at the cell surface as an ion
51 channel that is sensitive to mechanical cues (Beaulieu-Laroche et al., 2020). However, four
52 independent studies did not support such conclusion (Ke et al., 2021; Niu et al., 2021; Rong
53 et al., 2021; Xue et al., 2021). Instead, structural and biochemical analyses indicate that
54 TMEM120A forms a symmetrical homodimer and each protomer binds specifically to a
55 coenzyme-A (CoASH) molecule (Niu et al., 2021; Rong et al., 2021; Xue et al., 2021). These

56 observations led to the proposal that TMEM120A has an undefined role in lipid metabolism,
57 which correlates with its requirement for adipogenesis (Batrakou et al., 2015; Czapiewski et
58 al., 2021).

59 We identified mutant worms that were deficient of the sole *C. elegans* ortholog of
60 TMEM120A from an unbiased forward genetic screen. Here, we present evidence that *C.*
61 *elegans* TMEM-120 acts at the ER to promote TAG synthesis.

62 **Results and Discussion**

63 **TMEM-120 is required for TAG accumulation and LD expansion**

64 We have previously shown that lipid droplets (LDs) undergo continuous expansion in
65 *C. elegans daf-22*/thiolase mutant worms, owing to a block in the peroxisomal β -oxidation
66 pathway (Zhang et al., 2010). These worms accumulate more triacylglycerol (TAG), which is
67 synthesized by the concerted action of ACS-22/acyl-CoA synthetase and DGAT-
68 2/diacylglycerol acyltransferase (Xu et al., 2012). Accordingly, loss of *acs-22* or *dgat-2*
69 function attenuates LD expansion of *daf-22* mutant worms. In a genetic screen for additional
70 *daf-22* suppressors, we identified a complementation group that consisted of two recessive
71 alleles, *hj49* and *hj50*. Molecular cloning revealed lesions in a gene annotated as M01G5.3,
72 hereafter named *tmem-120*, which encodes a predicted transmembrane protein that is
73 homologous to mammalian TMEM120A and TMEM120B (Batrakou et al., 2015) (Fig. S1A).
74 The *hj50* nonsense allele (Glutamine 290 to amber) caused ~90% reduction of *tmem-120*
75 mRNA level (Fig. S1A-B), possibly due to nonsense mediated decay. Therefore, it is a strong
76 loss of function allele. The *hj49* missense allele caused the substitution of a conserved
77 Glycine to Glutamate (G195E) (Fig. S1A). Based on the recently determined structures of
78 TMEM120A, this conserved Glycine residue locates in a flexible linker immediately N-
79 terminal to a coenzyme-A (CoASH) binding site (Niu et al., 2021; Rong et al., 2021; Xue et
80 al., 2021). Therefore, its replacement with Glutamate may alter the conformation of the linker
81 and in turn affect the orientation of residues that constitute the CoASH binding site (including
82 W193 of human TMEM120A and W197 of *C. elegans* TMEM-120). Since the phenotypes of
83 mutant worms carrying *hj49* and *hj50* were indistinguishable (Fig. S1C-E), we concluded that
84 the G195E substitution severely compromised TMEM-120 function. In subsequent
85 experiments, we used worms carrying the *hj50* nonsense allele for phenotypic analysis.

86 To visualize LDs of wild type and mutant animals, we used a recently developed
87 Stimulated Raman Scattering (SRS) microscopy system (Li et al., 2015). We focused on
88 detecting C-H bond vibration from TAG, which was highly concentrated in LDs. In
89 agreement with previous results based on the use of vital dye or fluorescent protein markers
90 (Xu et al., 2012), LDs in *daf-22* mutant worms were larger than those in wild type worms
91 (Fig. 1A). The loss of TMEM-120 function reduced LD size and blocked LD expansion in
92 wild type and *daf-22* mutant worms (Fig. 1A and C). Similar results were observed when we
93 used DHS-3::mRuby as a fluorescent LD marker (Zeng et al., 2020) (Fig. 1F). Next, we
94 quantified SRS signals, which were proportional to TAG content (Wang et al., 2011). We
95 detected 23% more SRS signals in *daf-22* mutant than wild type worms (Fig. 1B and D). In
96 contrast, *tmem-120* and *daf-22; tmem-120* mutant worms have 26% and 14% less SRS signals
97 than wild type worms, respectively (Fig. 1B and D). To complement our imaging approach,
98 we used liquid chromatography-mass spectrometry (LC-MS) to determine that *tmem-120*
99 mutant worms had almost 40% less TAG than wild type worms (Fig. 1E). Such reduction of
100 TAG was unlikely due to an alteration of feeding rate (Fig. S1F). Taken together, our results
101 indicate that TMEM-120 supports TAG accumulation and LD expansion.

102 Next, we sought to determine if mouse TMEM120A plays a conserved role in
103 regulating fat storage, even though it was reported to be a mechanosensory channel
104 (Beaulieu-Laroche et al., 2020). To this end, we expressed mouse TMEM120A in *daf-22;*
105 *tmem-120* mutant worms. We found that TMEM120A could rescue the LD phenotype in a
106 similar manner as *C. elegans* TMEM-120 (Fig. 1F). As a result, large LDs re-appeared in
107 intestinal cells of *daf-22; tmem-120* mutant worms. Therefore, we conclude that TMEM-120
108 and TMEM120A share a deeply conserved function of regulating cellular fat storage.

109

110 **TMEM-120 promotes the incorporation of fatty acids into TAG**

111 The cellular neutral lipid homeostasis is dependent on a balance between TAG
112 synthesis and mobilization at LDs. The TAG synthesis in turn relies on the availability of
113 dietary or de novo synthesized fatty acids. We sought to determine if the decrease in neutral
114 lipid content was caused by a decrease in TAG accumulation or accelerated TAG
115 mobilization by lipolysis in *tmem-120* mutant worms. To differentiate these possibilities, we
116 used Stimulated Raman Scattering (SRS) to detect exogenously supplied deuterium-labeled
117 fatty acids (Fu et al., 2014; Li et al., 2019). We tuned our system to detect C-D bond
118 vibrations to avoid the interference from endogenous fatty acids. To measure TAG
119 accumulation, we fed young adult wild type and mutant worms with deuterium-labeled
120 monounsaturated oleic acid (OA-d₃₄) and imaged live worms by SRS at regular intervals over
121 a period of 30 hours (Fig. 2A). We detected progressive increase of SRS signals from LDs in
122 both strains tested (Fig. 2C). However, the rate of increase in *tmem-120* worms was
123 significantly slower than that in wild type worms (Fig. 2E). Similar observations were made
124 when worms were fed deuterium-labeled saturated palmitic acid (PA-d₃₁) (Fig. S2A, C and
125 E). We conclude that loss of TMEM-120 function impairs the incorporation of exogenous
126 fatty acids into TAG.

127 To measure lipolysis, we fed newly hatched larval stage L1 worms with deuterium-
128 labeled monounsaturated oleic acid (OA-d₃₄) until they reached the young adult stage. We
129 then removed labeled fatty acids from the diet of these animals and imaged them by SRS at
130 regular intervals (Fig. 2B). The dissipation of SRS signals over time reflected the rate of
131 lipolysis, as the labeled fatty acids stored as TAG in LDs were metabolized. We found that
132 the rate of decrease of SRS signals was not significantly different between wild type and
133 *tmem-120* mutant worms (Fig. 2D and F). Similar observations were made when worms were
134 fed with saturated palmitic acid (PA-d₃₁) (Fig. S2B, D and F). We conclude that lipolysis is

135 not altered in *tmem-120* mutant worms. Taken together, our results indicate that the reduction
136 of neutral lipid content in these animals was primarily due to the retardation of fatty acid
137 incorporation into TAG.

138

139 **TMEM-120 is an ER resident protein**

140 Based on TOPCONS analysis (Tsirigos et al., 2015), the *C. elegans* TMEM-120 and
141 its human orthologs share the same predicted membrane topology, with their N- and C-
142 termini facing the cytoplasm (Fig. 3A). According to its cryo-EM structure, membrane
143 embedded TMEM120A has 6 transmembrane helices and forms homodimers (Ke et al., 2021;
144 Niu et al., 2021; Rong et al., 2021; Xue et al., 2021). Intriguing, a consensus has yet to
145 emerge regarding the subcellular localization of TMEM120A. Mammalian TMEM120A was
146 previously reported to reside at the nuclear envelope (Batrakou et al., 2015) or the
147 endoplasmic reticulum (ER) (Cho et al., 2020). In contrast, the assignment of TMEM120A as
148 a mechanosensory channel placed it at the plasma membrane (Beaulieu-Laroche et al., 2020).
149 We sought to determine the localization of *C. elegans* TMEM-120 when it was expressed at
150 the endogenous level in live animals. To this end, we used CRISPR mediated genome editing
151 (Arribere et al., 2014) to insert the coding sequence of the green fluorescent protein (GFP)
152 into the endogenous *tmem-120* locus (Fig. 3B). We generated two independent knockin
153 alleles, *hj239* and *hj270* (Fig. 3B). In one strain, GFP was fused to the N-terminus of TMEM-
154 120 via a flexible linker. In a second strain, GFP was expressed as part of the predicted C-
155 terminal cytoplasmic tail, leaving the extreme C-terminus unaltered. This design was
156 necessitated by the presence of a KxHxx motif at the C-terminus of TMEM-120, which could
157 function similarly as the KxKxx motif for ER retention (Jackson et al., 1990; Ma and
158 Goldberg, 2013). Both TMEM-120 fusion proteins were functional because their expression

159 did not significantly alter the lipid content of *daf-22* mutant worms, as observed when the
160 function of TMEM-120 was lost (Fig. S3A-B). We used established markers of intestinal ER
161 and LDs to ascertain the localization of TMEM-120 (Fig. 3C-D) and found that it co-
162 localized extensively with the ER marker.

163 Next, we determined the localization of TMEM-120(G195E) by inserting the GFP
164 coding sequence into the 5' end of *tmem-120(hj49)*. We found that GFP::TMEM-
165 120(G195E) was expressed at a comparable level as the wild type protein and localized
166 correctly to the ER (Fig. S3C). Therefore, we conclude that the G195E mutation most likely
167 attenuates TMEM-120 function as predicted from the TMEM120A structure.

168 Finally, we experimentally verified the location of the N- and C-terminal tails of
169 TMEM-120. To this end, we took advantage of the anti-GFP nanobody (vhhGFP4) directed
170 protein degradation system (Wang et al., 2017). By expressing a GFP nanobody::ZIF-1
171 fusion protein in the intestinal cytoplasm, GFP fusion proteins with the GFP moiety exposed
172 in the cytoplasm are subject to degradation (Fig. 3E). However, if the GFP moiety is in the
173 ER lumen, the fusion protein is protected. Indeed, we detected fluorescence signals from a
174 luminal ER GFP marker (*hjSi528*), even when GFP nanobody::ZIF-1 was co-expressed in the
175 same worm (Fig. 3F). In contrast, the two versions of GFP fusion protein with TMEM-120
176 were subject to degradation, when GFP nanobody::ZIF-1 was co-expressed in the intestine
177 (Fig. 3F). As a control, hypodermal GFP fusions with TMEM-120 remained detectable (Fig.
178 3F), indicating that anti-GFP nanobody directed, post-translational degradation was tissue-
179 restricted as designed. Taken together, our results firmly suggest that TMEM-120 is an ER
180 resident protein, with its N- and C-termini facing the cytoplasm.

181

182

183 **TMEM-120 regulates LD expansion cell autonomously**

184 We generated an additional *tmem-120* deletion allele, *hj281*, using CRISPR mediated
185 genome editing and Cre-LoxP mediated germline excision. Similar to the *hj50* allele, the
186 *hj281* allele conferred *tmem-120* loss of function phenotypes and suppressed LD expansion in
187 *daf-22* mutant worms (Fig. S3D-E). Re-expression of *tmem-120* in the intestine alone from a
188 single-copy transgene (*hjSi557*) was sufficient to support LD expansion in *daf-22(-); tmem-*
189 *120(hj281)* worms (Fig. S3D-E). Therefore, we conclude that TMEM-120 acts cell
190 autonomously to promote LD expansion in *C. elegans*.

191

192 **TMEM120 promotes adipogenesis in mammalian cells**

193 The expression level of TMEM120A and TMEM120B is induced during the
194 differentiation of 3T3-L1 pre-adipocytes into adipocytes (Batrakou et al., 2015). In addition,
195 knockdown of TMEM120A and TMEM120B impedes the differentiation of 3T3-L1 pre-
196 adipocytes (Batrakou et al., 2015). To extend these observations, we used an alternative
197 model of adipogenesis: the murine OP9 pre-adipocytes (Wolins et al., 2006). In the presence
198 of insulin and oleic acid, the OP9 pre-adipocytes could differentiate into adipocytes in 3 days,
199 which was accompanied by the induction of adipocyte markers such as Glut4 and adiponectin
200 (Fig. S4A-B). Over the same time course, the expression level of TMEM120A and
201 TMEM120B was significantly increased (Fig. 4A-B). Next, we stably knocked down the
202 expression of TMEM120A and/or TMEM120B in OP9 cells by CRISPRi (Gilbert et al.,
203 2013) (Fig. S4C-D). Wild type and knockdown cells were induced to differentiate and mature
204 adipocytes were recognized by the appearance of a single, dominant LD (>15 μ m), as
205 visualized by Oil Red O staining (Fig. 4C-D). Consistent with previous observations in 3T3-
206 L1 cells, knockdown of TMEM120A and/or TMEM120B significantly reduced the ability of

207 OP9 cells to differentiate into adipocytes (Fig. 4C-D). Our results suggest that the two
208 mammalian TMEM120 paralogs are required for adipogenesis in vitro.

209

210 **TMEM120 promotes LD expansion in mammalian cells**

211 Next, we tested if TMEM120A was sufficient to promote LD expansion in
212 mammalian COS7 cells. To this end, we generated COS7 cells that stably over-expressed
213 TMEM120A using the Sleeping Beauty Transposon system (Kowarz et al., 2015). When
214 oleic acid was added to induce LD expansion, we observed significantly larger LDs in cells
215 that over-expressed TMEM120A in comparison to parental cells (Fig. 4E-F). Therefore,
216 TMEM120A is sufficient to promote LD expansion, plausibly by elevating the amount of
217 fatty acids that are available for the synthesis of TAG, which is stored in LDs. It should be
218 noted that excess fatty acids that cannot be incorporated into TAG, are toxic to cells. As a
219 result, cell death ensues (Listenberger et al., 2003). Accordingly, COS7 cells that over-
220 expressed TMEM120A are more sensitive than parental cells to inhibitors of diacylglycerol
221 acyltransferase 1 (DGAT1) in the presence of exogenous fatty acids (Fig. 4G-J, S4E-F).
222 Almost all cells that over-expressed TMEM120A died when oleic or palmitic acid was
223 applied simultaneously with the DGAT1 inhibitor A922500. Interestingly, the dose-sensitive
224 response to DGAT1 inhibitors was not observed for a diacylglycerol acyltransferase 2
225 (DGAT2) inhibitor (Fig. S4G). Based on the current model of LD biogenesis and expansion
226 (Cao and Mak, 2020; Olzmann and Carvalho, 2019), DGAT1 in the ER acts early to
227 synthesize TAG that supports the emergence of LDs from the ER while LD-localized
228 DGAT2 contributes more significantly to the expansion of mature LDs. Our results on the
229 differential sensitivity of TMEM120A over-expressing cells to DGAT1 inhibitors are

230 consistent with the notion that TMEM120A acts in the ER to promote the incorporation of
231 fatty acids into TAG, upstream of DGAT1.

232

233 **Concluding remarks**

234 In this paper, we combined genetic, imaging and pharmacological approaches to
235 demonstrate an evolutionarily conserved function of TMEM-120/TMEM120A in promoting
236 TAG synthesis and LD expansion. Our examination of TMEM-120 at the endogenous level
237 in live worms strongly suggests the ER as its primary site of action. This is consistent with
238 the notion that the ensemble of TAG synthesis proteins can all be found in the ER, which
239 conceivably enables the transfer of biosynthetic intermediates within the membrane.

240 Although we do not yet know if TMEM-120/TMEM120A acts specifically with one or more
241 enzymes in the TAG synthesis pathway, the ability of purified TMEM120A to bind CoASH
242 is intriguing (Niu et al., 2021; Rong et al., 2021; Xue et al., 2021). This is because fatty acids
243 are converted to fatty acyl-CoA by acyl-CoA synthetases, prior to their addition to the
244 glycerol backbone by a series of acyltransferases (Coleman and Lee, 2004; Yen et al., 2008).

245 We note that TMEM-120 mutant worms remain capable of TAG synthesis, albeit at a
246 reduced level (Fig. 1E). It is plausible that TMEM-120/TMEM120A can trap CoASH or
247 acyl-CoA in the ER to enhance the efficiency of TAG synthesis. Such hypothesis can be
248 tested with purified proteins and substrates in vitro. In conclusion, our functional studies in *C.*
249 *elegans* and mammalian cells support the conclusion from structural studies that TMEM120A
250 and its orthologs are unlikely to be mechanosensory channels.

251 **Materials and Methods**

252 **Strains and transgenes**

253 The wide type *C. elegans* strain was Bristol N2. All experimental animals were maintained at
254 20°C. The following strains and alleles were used: LG I, EG6701 (*ttTi4348*); LG II, *daf-22*
255 (*ok693*); LG III, *tmem-120(h49)*, *tmem-120(hj50)*; LG IV, EG6703 (*cxTi10816*).

256 The following transgenes or CRISPR-generated alleles were used:

257 *hjSi158* [*vha-6p::sel-1(a.a.1-79)::mCherry::HDEL::let-858 3'UTR*] I

258 *hjSi524* [*vha-6p::vhhgfp4::zif-1::let-858 3'UTR*] I

259 *hjSi528* [*vha-6p::sel-1(a.a.1-79)::GFP::HDEL::tbb-2 3'UTR*] IV

260 *hjSi557* [*vha-6p::gfp::3xFLAG::tmem-120(codon modified) cDNA::dhs-28 3'-UTR*] IV

261 *dhs-3 (hj200)* [*dhs-3::mRuby*] I

262 *tmem-120 (hj239)* [*tmem-120(a.a.1-368)::gfp::3xFLAG::tmem-120(a.a.369 to stop)*] III

263 *tmem-120 (hj266)* [*tmem-120(a.a.1-368)(loxP in introns 3 and 4)::gfp::3xFLAG::tmem-*
264 *120(a.a.369 to stop)*] III

265 *tmem-120 (hj270)* [*GFP::3xFLAG::tmem-120*] III

266 *tmem-120 (hj297)* [*GFP::3xFLAG::TMEM-120(G195E)*] III

267 The *tmem-120(hj281)* allele was generated by Cre-loxP mediated germline excision of *tmem-*
268 *120(hj266)*.

269 Extrachromosomal array strains:

270 *hjEx29*[*vha-6p::tmem-120 cDNA::sl2::gfp::let-858 3' UTR*]

271 *hjEx30*[*vha-6p::mouse tmem120a cDNA::sl2::gfp::let-858 3'UTR*]

272 All strains were outcrossed with wild type N2 at least twice before further characterization.

273

274

275 **Genetic screen**

276 The *tmem-120* alleles were isolated in a genetic screen for suppressors of the expanded LD
277 phenotype of *daf-22(ok693)* mutants. Complementation tests indicated that *hj49* and *hj50*
278 belonged to the same complementation group. Using a SNP-based mapping strategy with the
279 Hawaiian *C. elegans* isolate CB4856 (Davis et al., 2005), we mapped *hj50* to LGIII. Mutant
280 worms were then subjected to whole genome sequencing (Illumina). The molecular lesions of
281 *hj49* and *hj50* in M01G5.3 were confirmed by Sanger sequencing. The *daf-22(ok693); tmem-*
282 *120(hj50)* mutant could be rescued by a *vha-6p::tmem-120::sl2::gfp* transgene (Fig. 1F).

283

284 **Fluorescence Imaging of *C. elegans* and mammalian cells**

285 Fluorescence imaging of live worms and mammalian cells was performed as described (Cao
286 et al., 2019). In brief, fluorescence images of worms at indicated stages were acquired on a
287 spinning disk confocal microscope (AxioObserver Z1, Carl Zeiss) equipped with a piezo Z
288 stage using a 63x, NA 1.4 (for visualizing TMEM-120 localization) or 100x, NA 1.46 (for
289 quantification of LD diameter) oil Alpha-Plan-Apochromat objective on a Neo sCMOS
290 camera (Andor) controlled by the iQ3 software (Andor). For GFP, a 488nm laser was used
291 for excitation and signals were collected with a 500-550nm emission filter. For mRuby or
292 mCherry, a 561nm laser was used for excitation and signals were collected with a 580.5-
293 653.5nm emission filter. For autofluorescence from lysosome-related organelles, a 488nm
294 laser was used for excitation and signals were collected with a 580.5-653.5nm emission filter.
295 For BFP, a 405 nm laser was used for excitation, and signals were collected with a 437nm
296 emission filter. For FAS LD dye, a 405nm laser was used for excitation and signals were
297 collected with a 617nm emission filter. Optical sections, as specified, were taken at 0.5 μ m

298 intervals and z stacks of 8 μ m-10 μ m were exported from iQ3 to Imaris 8 (Bitplane) for
299 processing.

300

301 **Live imaging by Stimulated Raman Scattering**

302 Stimulated Raman Scattering (SRS) for measuring endogenous neutral lipid in live worms
303 was carried out as described (Li et al., 2015). Live animals at specific stages were mounted
304 on 8% agarose pad in 1xPBS buffer with 0.2mM levamisole. For visualizing LDs, the focal
305 plane for the center of the first and second intestinal segments in young adult animals was
306 determined with a 40x water immersion objective (UAPO40XW3/340, 1.15 NA, Olympus).
307 To measure neutral lipid content level in whole worms, the focal plane with maximal SRS
308 intensity was determined with a 20x air objective (Plan-Apochromat, 0.8 NA, Zeiss). The C-
309 H bond was detected at 2863.5 cm^{-1} . The quantification of SRS signal was done following a
310 published protocol (Ramachandran et al., 2015). SRS of live worms for measuring fatty acid
311 absorption and lipolysis were carried out as described with a 40x water immersion objective
312 (UAPO40XW3/340, 1.15 NA, Olympus) (Li et al., 2019). Saturated bacterial cultures of
313 OP50 were mixed with 4mM deuterium labeled PA-d₃₁ or OA-d₃₄ (Sigma) and then seeded
314 onto NGM plates. To measure fatty acid uptake, populations of young adult worms (before
315 egg-laying started), raised in the absence of deuterium labeled fatty acid were transferred to
316 plates with PA-d₃₁ or OA-d₃₄. To measure lipolysis, populations of L1 larvae were raised on
317 plates with PA-d₃₁ or OA-d₃₄, and transferred to OP50 seeded plates without deuterium
318 labeled fatty acid when they were young adults. Animals were imaged by SRS at 5 to 6-hour
319 intervals for 28 to 30 hours. The C-D bond vibration was detected at 2116.8 cm^{-1} . Images
320 were imported into ImageJ and further processed for quantification in MATLAB_R2015a.

321

322 **Real-time PCR for *C. elegans* samples**

323 For each experimental sample, around 400 worms were synchronized at the L1 larval stage.
324 Worms were harvested at the L4 stage (43 hours after L1 for WT, and 46 hours after L1 for
325 *tmem-120(hj50)*), and total RNA extracted with a Direct-zol™ RNA MiniPrep kit (Zymo).
326 200ng of total RNA was reverse transcribed with a Transcriptor cDNA synthesis kit (Roche).
327 The real time PCR was carried out on a Roche LightCycler system with SYBR Green Master
328 Mix (Roche). For each strain, technical triplicates were performed for each biological
329 sample. The Delta-delta CT method was used for analyzing the raw CT values.

330 The following primers were used for RT-qPCR:

331 For *tmem-120*:

332 Forward: 5'-TGAGACAAGCCCAACAATCA-3'

333 Reverse: 5'-TGGAGCCCAAATCAAATTC-3'

334 For internal standard *rpl-32*:

335 Forward: 5'-AGGGAATTGATAACCGTGTCCGCA-3'

336 Reverse: 5'-TGTAGGACTGCATGAGGAGCATGT-3'

337

338 **Real-time PCR of mammalian samples**

339 Total RNA was extracted from mammalian cells using Direct-zol™ RNA MiniPrep kit
340 (Zymo) following the manufacturer's protocol. 500ng of total RNA was reverse transcribed
341 using First Strand cDNA Synthesis Kit (Sigma Aldrich) following the manufacturer's
342 protocol. The real time PCR was performed on a LightCycler480 system (Roche) using
343 SYBR Green Master Mix (Roche) following the manufacturer's protocol. Data was obtained
344 with 3 biological samples of each cell line, tested in technical triplicates. The Delta-delta CT
345 method was used for analyzing the raw CT values.

346 The following primers were used:

347 For TMEM120A:

348 Forward: 5'-AGGGCTTTCAGTCTTGGATG-3'

349 Reverse: 5'-AAATTGCCGAGGAAGAGGAG-3'

350 For TMEM120B:

351 Forward: 5'-TCAGAGCTGCGTTCAGTTTC-3'

352 Reverse: 5'-ACAGAAGAGGAAAGGCAGGAG-3'

353 For Glut4:

354 Forward: 5'-GTA ACTTCATTGTCGGCATGG-3'

355 Reverse: 5'-CTCTGGTTTCAGGCACTTTTAG-3'

356 For Adiponectin:

357 Forward: 5'-CCTGGCCACTTTCTCCTC-3'

358 Reverse: 5'-GTGGAGGGACCAAAGCAG-3'

359 For 36B4 (internal control) (Zhang et al., 2016):

360 Forward: 5'-CTGAGTGATGTGCAGCTGAT-3'

361 Reverse: 5'-AGAAGGGGGAGATGTTTCAG-3'

362

363 **Pharyngeal pumping rate**

364 Videos for pharyngeal pumping rate measurement were obtained on an OLYMPUS SZX16
365 stereo microscope. One day before the imaging, L4 stage worms were transferred to a newly
366 seeded NGM plate. The plates were left beside the microscope for acclimatization. For each
367 experimental group, up to 10 worms were prepared. A 2-minute video focusing on the
368 pharynx of each worm was captured. Each video was trimmed to a 60 seconds clip and then
369 played under 0.3X speed for counting the number of pharyngeal contractions visually.

370

371 **Lipid analysis**

372 Lipid extraction was conducted using methyl-tert-butyl ether(MTBE) as described (Matyash
373 et al., 2008; Witting et al., 2014), with modifications. For each experimental sample, around
374 2,000 worms were synchronized at L1 larvae stage. Worms were harvested at the L4 stage
375 (43 hours after L1 for WT, and 46 hours after L1 for *tmem-120(hj50)*), washed with detergent
376 free PBS for at least three times and transferred into organic solvent resistant Eppendorf
377 tubes. 250µl methanol (precooled to -20°C) (RDH, for HPLC) was added and samples were
378 frozen in liquid nitrogen and stored at -80°C. For extraction, samples were thawed on ice, and
379 875µl MTBE (VWR, for HPLC) was added. Worms were lysed with ice cold ultrasonic bath
380 with an interval of 2 mins on and 30 seconds off. Phase separation was induced by the
381 addition of 210µl water with further sonication for 15 mins. After centrifugation at 16,100xG
382 at 4°C for 15 mins, the upper organic phase was collected into a glass vial. 325µl MTBE was
383 added to the lower phase and centrifuged at 17,000xG at 4°C for 15 mins for re-extraction of
384 lipids. Upper organic phase was collected after centrifugation and combined with those
385 previously collected. Extracts were dried under a stream of nitrogen at room temperature, re-
386 dissolved in 200µl acetonitrile (RCI Labscan, for HPLC)/ isopropanol (RNH)/ water(65/30/5,
387 v/v/v) and stored at -80 °C.

388 Lipid analysis was performed as previously described (Zeng et al., 2020). A 100µl aliquot
389 was analyzed using the Bruker Elute UPLC system with 2 technical injections per sample.
390 The mass spectrometry data was analyzed with MetaboScape version 5.0, annotated with
391 spectral libraries MSDIAL- Tandem Mass Spectral Atlas-VS68-pos and MSDIAL- Tandem
392 Mass 736 Spectral Atlas-VS68-neg. The intensity was normalized with probabilistic quotient
393 normalization method (Dieterle et al., 2006). Signals from all TAG species were summed.

394

395 **Cell culture**

396 OP9 mouse stromal cells (ATCC-CRL-2749) were maintained in α -MEM (Life
397 Technologies) with 20% FBS (Life Technologies) and 1% antibiotic-antimycotic (Life
398 Technologies). COS7 Cells (ATCC-CRL-1651) were maintained in DMEM (Life
399 Technologies) with 10% FBS (Life Technologies) and 1% antibiotic-antimycotic (Life
400 Technologies). All the cell lines were incubated in 37°C humidified incubator with 5% CO₂.

401

402 **Generation of TMEM120A overexpressing COS7 cells**

403 The Sleeping beauty transposon system was used to generate COS7 cells that overexpressed
404 human TMEM120A. Cells were co-transfected with sleeping beauty transposon plasmid
405 pSBi-Hyg-BFP (hTMEM120A cDNA) and sleeping beauty transposase plasmid pCMV
406 (CAT) T7-SB100 with Lipofectamine2000 (Life Technologies). Three days after
407 transfection, cells were maintained in selection medium (400 μ g/mL hygromycin in DMEM
408 growth medium) for at least seven days. Cells that survived drug selection were sorted using
409 Aria III system (Becton Dickinson) and sub-divided into 'Low', 'Medium', and 'High'
410 populations based on BFP fluorescence intensity (a surrogate of TMEM120A expression).
411 The 'High' cell population was used in subsequent experiments.

412

413 **Generation of TMEM120A and TMEM120B knockdown OP9 cells**

414 OP9 cells were co-transfected with the sleeping beauty transposase plasmid pCMV (CAT)
415 T7-SB100 and the transposon plasmid (Krab::dCas9::BFP::TMEM120A sgRNA or
416 TMEM120B sgRNA). The sgRNA sequences were selected from a published database
417 (Horlbeck et al., 2016). The transfected cells were maintained in selection medium
418 (400 μ g/mL hygromycin in α -MEM growth medium) for at least seven days. Cells that

419 survived drug selection were sorted into ‘Low’, ‘Medium’, and ‘High’ populations based on
420 the BFP fluorescence intensity (a surrogate of dCas9 and sgRNA expression). The ‘Medium’
421 cell populations were used for subsequent experiments.

422 For the TMEM120A+TMEM120B double knockdown cells, the sleeping beauty transposase
423 plasmid and the transposon plasmid (mRuby::TMEM120B sgRNA) were transfected into
424 TMEM120A knockdown cells. Drug selection and cell sorting were performed as described
425 above except that puromycin was used instead of hygromycin. The ‘High’ cell population
426 was used for subsequent experiments. The knockdown efficiency of all stable cell lines was
427 determined by real time PCR.

428

429 **Fatty acid supplementation**

430 Fatty acids supplementation was performed according to a published method (Cao et al.,
431 2019; Peng et al., 2011). In brief, the cell culture medium was pre-heated to 60°C for 5 mins
432 prior to the addition of fatty acids (400µM oleic acid or palmitic acid). The medium was then
433 equilibrated to 37°C before use. To induce LD expansion, cells were incubated with 400µM
434 FAs for 20 hours. To visualize LDs, the cells were stained with 10µM FAS (Wang et al.,
435 2016) for 15 mins prior to imaging.

436

437 **DGAT inhibitor and fatty acids treatment**

438 The cell culture medium was pre-heated to 60°C for 5 mins prior to the addition of fatty acids
439 (400µM oleic acid or 400µM palmitic acid or ethanol control), without (DMSO control) or
440 with DGAT inhibitors as specified (A922500, PF04620110 or PF 06424439 (R&D system)).
441 The medium was equilibrated to 37°C before use. The cells were treated with 20 hours (oleic

442 acid) or 60 hours (palmitic acid) before they were stained with crystal violet. Quantification
443 of crystal violet was performed according to a published protocol (Feoktistova et al., 2016).

444 **Author Contributions**

445 Y.L. was responsible for Figs. 1, 2, 3, S1 (except S1F), S2 and S3. S.H. was responsible for
446 Figs. 4 and S4. X.L. and J.Q. were responsible for developing the SRS system and Figs. 1A-
447 B, 2 and S2. X.Y. was responsible for Fig. S1F and the generation of *tmem-120(hj266)*,
448 *tmem-120(hj281)* and *hjSi557*. N.X. conducted genetic screen, genetic mapping and
449 molecular cloning of *C. elegans* mutants. H.Y.M. supervised the project and wrote the paper.

450

451 **Acknowledgements**

452 We thank Yifei Qiu for preliminary data, Zhenfeng Liu for discussion, Pui Shuen Wong at
453 the HKUST Bioscience Central Research Facility for lipidomic analysis, the Molecular
454 Biology core at the Stowers Institute for Medical Research for whole-genome sequencing.
455 Some strains were provided by the CGC, which is funded by NIH Office of Research
456 Infrastructure Programs (P40 OD010440). This work was supported by RGC GRF 662013 to
457 HYM.

458

459 **Competing interests**

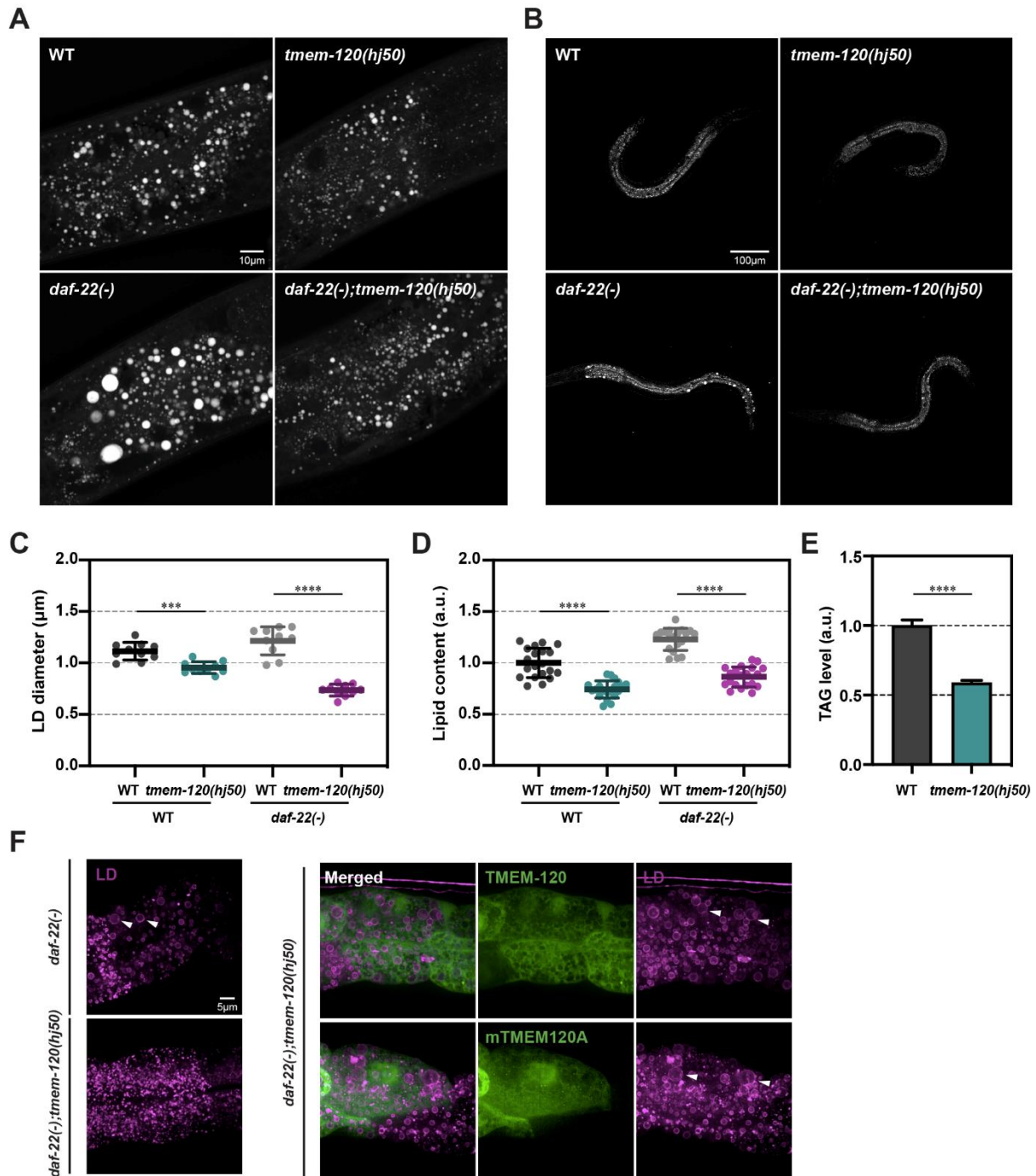
460 The authors declare no competing interest.

461 References

- 462 Arribere JA, Bell RT, Fu BXH, Artiles KL, Hartman PS, Fire AZ. 2014. Efficient marker-
463 free recovery of custom genetic modifications with CRISPR/Cas9 in *Caenorhabditis*
464 *elegans*. *Genetics* **198**:837–846. doi:10.1534/genetics.114.169730
- 465 Batrakou DG, de Las Heras JI, Czapiewski R, Mouras R, Schirmer EC. 2015. TMEM120A
466 and B: Nuclear Envelope Transmembrane Proteins Important for Adipocyte
467 Differentiation. *PLoS One* **10**:e0127712. doi:10.1371/journal.pone.0127712
- 468 Beaulieu-Laroche L, Christin M, Donoghue A, Agosti F, Yousefpour N, Petitjean H,
469 Davidova A, Stanton C, Khan U, Dietz C, Faure E, Fatima T, MacPherson A,
470 Mouchbahani-Constance S, Bisson DG, Haglund L, Ouellet JA, Stone LS, Samson J,
471 Smith M-J, Ask K, Ribeiro-da-Silva A, Blunck R, Poole K, Bourinet E, Sharif-Naeini
472 R. 2020. TACAN Is an Ion Channel Involved in Sensing Mechanical Pain. *Cell*
473 **180**:956–967.e17. doi:10.1016/j.cell.2020.01.033
- 474 Cao Z, Hao Y, Fung CW, Lee YY, Wang P, Li X, Xie K, Lam WJ, Qiu Y, Tang BZ, Shui G,
475 Liu P, Qu J, Kang B-H, Mak HY. 2019. Dietary fatty acids promote lipid droplet
476 diversity through seipin enrichment in an ER subdomain. *Nat Commun* **10**:2902.
477 doi:10.1038/s41467-019-10835-4
- 478 Cao Z, Mak HY. 2020. Married at Birth: Regulation of Cellular Fat Metabolism by ER–Lipid
479 Droplet Crosstalk. *Contact*. doi:10.1177/2515256420934671
- 480 Cho KF, Branon TC, Udeshi ND, Myers SA, Carr SA, Ting AY. 2020. Proximity labeling in
481 mammalian cells with TurboID and split-TurboID. *Nat Protoc* **15**:3971–3999.
482 doi:10.1038/s41596-020-0399-0
- 483 Coleman RA, Lee DP. 2004. Enzymes of triacylglycerol synthesis and their regulation. *Prog*
484 *Lipid Res* **43**:134–176.
- 485 Czapiewski R, Batrakou DG, de las Heras JI, Carter RN, Sivakumar A, Sliwinska M, Dixon
486 CR, Webb S, Lattanzi G, Morton NM, Schirmer EC. 2021. Genomic loci
487 mispositioning in *Tmem120a* knockout mice yields latent lipodystrophy.
488 *bioRxiv* 2021.04.12.439495. doi:10.1101/2021.04.12.439495
- 489 Davis MW, Hammarlund M, Harrach T, Hullett P, Olsen S, Jorgensen EM. 2005. Rapid
490 single nucleotide polymorphism mapping in *C. elegans*. *BMC Genomics* **6**:118.
491 doi:10.1186/1471-2164-6-118
- 492 Dieterle F, Ross A, Schlotterbeck G, Senn H. 2006. Probabilistic quotient normalization as
493 robust method to account for dilution of complex biological mixtures. Application in
494 1H NMR metabolomics. *Anal Chem* **78**:4281–4290. doi:10.1021/ac051632c
- 495 Feoktistova M, Geserick P, Leverkus M. 2016. Crystal Violet Assay for Determining
496 Viability of Cultured Cells. *Cold Spring Harb Protoc* **2016**:pdb.prot087379.
497 doi:10.1101/pdb.prot087379
- 498 Fu D, Yu Y, Folick A, Currie E, Farese RV, Tsai T-H, Xie XS, Wang MC. 2014. In vivo
499 metabolic fingerprinting of neutral lipids with hyperspectral stimulated Raman
500 scattering microscopy. *J Am Chem Soc* **136**:8820–8828. doi:10.1021/ja504199s
- 501 Gilbert LA, Larson MH, Morsut L, Liu Z, Brar GA, Torres SE, Stern-Ginossar N, Brandman
502 O, Whitehead EH, Doudna JA, Lim WA, Weissman JS, Qi LS. 2013. CRISPR-
503 mediated modular RNA-guided regulation of transcription in eukaryotes. *Cell*
504 **154**:442–451. doi:10.1016/j.cell.2013.06.044
- 505 Henne WM, Reese ML, Goodman JM. 2018. The assembly of lipid droplets and their roles in
506 challenged cells. *EMBO J* **37**:e98947. doi:10.15252/embj.201898947
- 507 Horlbeck MA, Gilbert LA, Villalta JE, Adamson B, Pak RA, Chen Y, Fields AP, Park CY,
508 Corn JE, Kampmann M, Weissman JS. 2016. Compact and highly active next-

- 509 generation libraries for CRISPR-mediated gene repression and activation. *eLife* **5**.
510 doi:10.7554/eLife.19760
- 511 Jackson MR, Nilsson T, Peterson PA. 1990. Identification of a consensus motif for retention
512 of transmembrane proteins in the endoplasmic reticulum. *EMBO J* **9**:3153–3162.
- 513 Ke M, Yu Y, Zhao C, Lai S, Su Q, Yuan W, Yang L, Deng D, Wu K, Zeng W, Geng J, Wu J,
514 Yan Z. 2021. Cryo-EM structures of human TMEM120A and TMEM120B. *bioRxiv*
515 2021.06.27.450060. doi:10.1101/2021.06.27.450060
- 516 Kowarz E, Löscher D, Marschalek R. 2015. Optimized Sleeping Beauty transposons rapidly
517 generate stable transgenic cell lines. *Biotechnol J* **10**:647–653.
518 doi:10.1002/biot.201400821
- 519 Li X, Lam WJ, Cao Z, Hao Y, Sun Q, He S, Mak HY, Qu JY. 2015. Integrated femtosecond
520 stimulated Raman scattering and two-photon fluorescence imaging of subcellular lipid
521 and vesicular structures. *J Biomed Opt* **20**:110501. doi:10.1117/1.JBO.20.11.110501
- 522 Li X, Li Y, Jiang M, Wu W, He S, Chen C, Qin Z, Tang BZ, Mak HY, Qu JY. 2019.
523 Quantitative Imaging of Lipid Synthesis and Lipolysis Dynamics in *Caenorhabditis*
524 *elegans* by Stimulated Raman Scattering Microscopy. *Anal Chem* **91**:2279–2287.
525 doi:10.1021/acs.analchem.8b04875
- 526 Listenberger LL, Han X, Lewis SE, Cases S, Farese RV, Ory DS, Schaffer JE. 2003.
527 Triglyceride accumulation protects against fatty acid-induced lipotoxicity. *Proc Natl*
528 *Acad Sci U S A* **100**:3077–3082. doi:10.1073/pnas.0630588100
- 529 Ma W, Goldberg J. 2013. Rules for the recognition of dilysine retrieval motifs by coatomer.
530 *EMBO J* **32**:926–937. doi:10.1038/emboj.2013.41
- 531 Matyash V, Liebisch G, Kurzchalia TV, Shevchenko A, Schwudke D. 2008. Lipid extraction
532 by methyl-tert-butyl ether for high-throughput lipidomics. *J Lipid Res* **49**:1137–1146.
533 doi:10.1194/jlr.D700041-JLR200
- 534 Niu Y, Tao X, Vaisey G, Olinares PDB, Alwaseem H, Chait BT, MacKinnon R. 2021.
535 Analysis of the Mechanosensor Channel Functionality of TACAN. *bioRxiv*
536 2021.06.11.448078. doi:10.1101/2021.06.11.448078
- 537 Olzmann JA, Carvalho P. 2019. Dynamics and functions of lipid droplets. *Nat Rev Mol Cell*
538 *Biol* **20**:137–155. doi:10.1038/s41580-018-0085-z
- 539 Peng G, Li L, Liu Y, Pu J, Zhang S, Yu J, Zhao J, Liu P. 2011. Oleate blocks palmitate-
540 induced abnormal lipid distribution, endoplasmic reticulum expansion and stress, and
541 insulin resistance in skeletal muscle. *Endocrinology* **152**:2206–2218.
542 doi:10.1210/en.2010-1369
- 543 Ramachandran PV, Mutlu AS, Wang MC. 2015. Label-free biomedical imaging of lipids by
544 stimulated Raman scattering microscopy. *Curr Protoc Mol Biol* **109**:30.3.1–17.
545 doi:10.1002/0471142727.mb3003s109
- 546 Rong Y, Jiang J, Gao Y, Guo J, Song D, Liu W, Zhao Y, Xiao B, Liu Z. 2021. TMEM120A
547 contains a specific coenzyme A-binding site and might not mediate poking- or stretch-
548 induced channel activities in cells. *bioRxiv* 2021.06.17.448797.
549 doi:10.1101/2021.06.17.448797
- 550 Schirmer EC, Florens L, Guan T, Yates JR, Gerace L. 2003. Nuclear membrane proteins with
551 potential disease links found by subtractive proteomics. *Science* **301**:1380–1382.
552 doi:10.1126/science.1088176
- 553 Schuldiner M, Bohnert M. 2017. A different kind of love - lipid droplet contact sites. *Biochim*
554 *Biophys Acta* **1862**:1188–1196. doi:10.1016/j.bbailip.2017.06.005
- 555 Thiam AR, Ikonen E. 2021. Lipid Droplet Nucleation. *Trends Cell Biol* **31**:108–118.
556 doi:10.1016/j.tcb.2020.11.006

- 557 Tsirigos KD, Peters C, Shu N, Käll L, Elofsson A. 2015. The TOPCONS web server for
558 consensus prediction of membrane protein topology and signal peptides. *Nucleic*
559 *Acids Res* **43**:W401-407. doi:10.1093/nar/gkv485
- 560 Walther TC, Chung J, Farese RV. 2017. Lipid Droplet Biogenesis. *Annu Rev Cell Dev Biol*
561 **33**:491–510. doi:10.1146/annurev-cellbio-100616-060608
- 562 Wang MC, Min W, Freudiger CW, Ruvkun G, Xie XS. 2011. RNAi screening for fat
563 regulatory genes with SRS microscopy. *Nat Methods* **8**:135–138.
564 doi:10.1038/nmeth.1556
- 565 Wang S, Tang NH, Lara-Gonzalez P, Zhao Z, Cheerambathur DK, Prevo B, Chisholm AD,
566 Desai A, Oegema K. 2017. A toolkit for GFP-mediated tissue-specific protein
567 degradation in *C. elegans*. *Dev Camb Engl* **144**:2694–2701. doi:10.1242/dev.150094
- 568 Wang Z, Gui C, Zhao E, Wang J, Li X, Qin A, Zhao Z, Yu Z, Tang BZ. 2016. Specific
569 Fluorescence Probes for Lipid Droplets Based on Simple AIEgens. *ACS Appl Mater*
570 *Interfaces* **8**:10193–10200. doi:10.1021/acsami.6b01282
- 571 Witting M, Maier TV, Garvis S, Schmitt-Kopplin P. 2014. Optimizing a ultrahigh pressure
572 liquid chromatography-time of flight-mass spectrometry approach using a novel sub-
573 2µm core-shell particle for in depth lipidomic profiling of *Caenorhabditis elegans*. *J*
574 *Chromatogr A* **1359**:91–99. doi:10.1016/j.chroma.2014.07.021
- 575 Wolins NE, Quaynor BK, Skinner JR, Tzekov A, Park C, Choi K, Bickel PE. 2006. OP9
576 mouse stromal cells rapidly differentiate into adipocytes: characterization of a useful
577 new model of adipogenesis. *J Lipid Res* **47**:450–460. doi:10.1194/jlr.D500037-
578 JLR200
- 579 Xu N, Zhang SO, Cole RA, McKinney SA, Guo F, Haas JT, Bobba S, Farese RV Jr, Mak
580 HY. 2012. The FATP1-DGAT2 complex facilitates lipid droplet expansion at the ER-
581 lipid droplet interface. *J Cell Biol* **198**:895–911. doi:10.1083/jcb.201201139
- 582 Xue J, Han Y, Baniyadi H, Zeng W, Pei J, Grishin N, Wang J, Tu BP, Jiang Y. 2021.
583 TMEM120 is a coenzyme A-binding membrane protein with structural similarities to
584 ELOVL fatty acid elongase. *bioRxiv* 2021.06.13.448233.
585 doi:10.1101/2021.06.13.448233
- 586 Yen C-LE, Stone SJ, Koliwad S, Harris C, Farese RV Jr. 2008. Thematic review series:
587 glycerolipids. DGAT enzymes and triacylglycerol biosynthesis. *J Lipid Res* **49**:2283–
588 2301. doi:10.1194/jlr.R800018-JLR200
- 589 Zeng L, Li X, Preusch CB, He GJ, Xu N, Cheung TH, Qu J, Mak HY. 2020. Nuclear receptor
590 NHR-49 promotes peroxisome proliferation to compensate for aldehyde
591 dehydrogenase deficiency in *C. elegans*. *bioRxiv* 2020.12.04.411637.
592 doi:10.1101/2020.12.04.411637
- 593 Zhang SO, Box AC, Xu N, Le Men J, Yu J, Guo F, Trimble R, Mak HY. 2010. Genetic and
594 dietary regulation of lipid droplet expansion in *Caenorhabditis elegans*. *Proc Natl*
595 *Acad Sci U S A* **107**:4640–4645. doi:10.1073/pnas.0912308107
- 596 Zhang W-X, Fan J, Ma J, Rao Y-S, Zhang L, Yan Y-E. 2016. Selection of Suitable Reference
597 Genes for Quantitative Real-Time PCR Normalization in Three Types of Rat Adipose
598 Tissue. *Int J Mol Sci* **17**:E968. doi:10.3390/ijms17060968
599

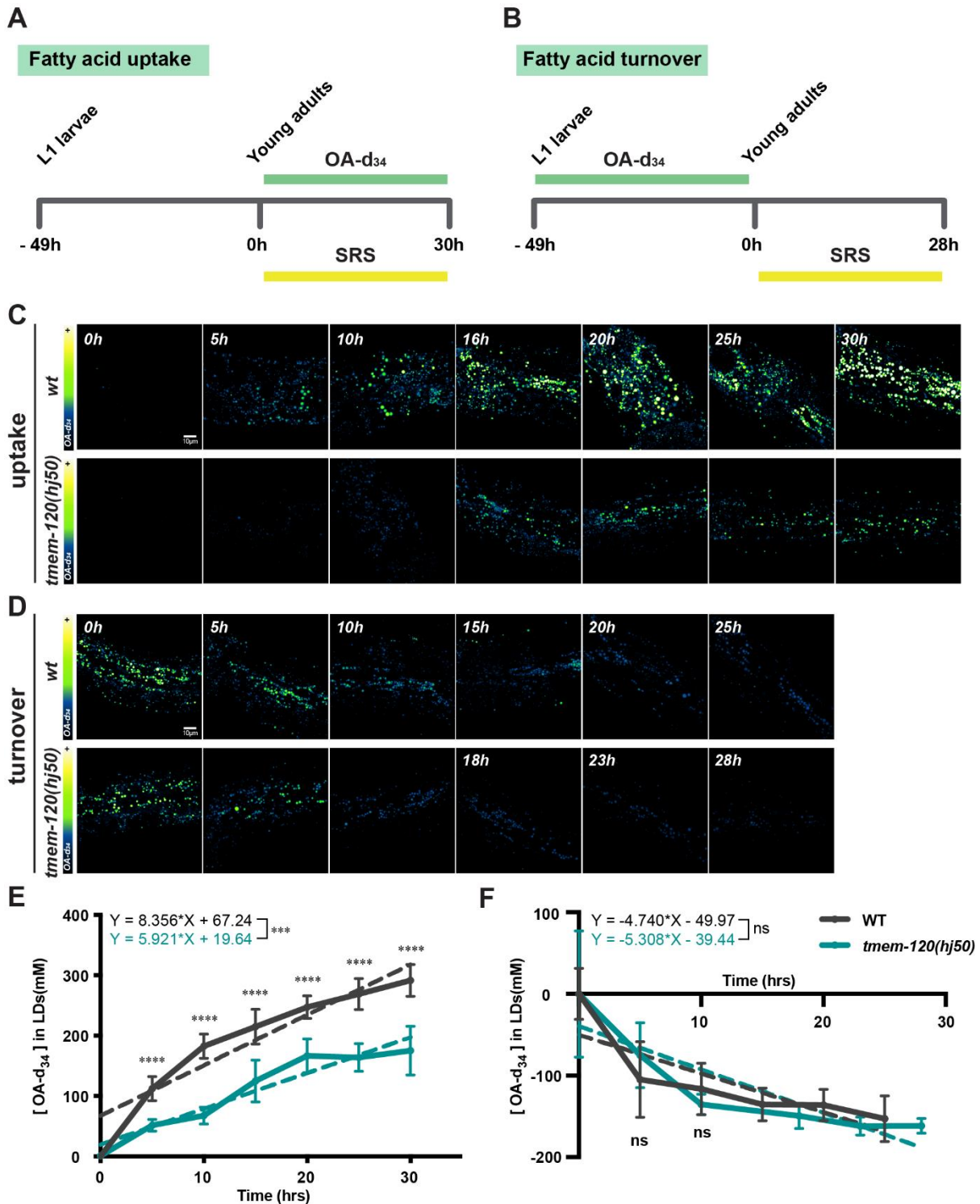


600

601 **Figure 1. TMEM-120 promotes TAG synthesis and LD expansion.** (A) Visualization of
 602 LDs in wild type (WT), *tmem-120(hj50)*, *daf-22(ok693)* and *daf-22(ok693); tmem-120(hj50)*
 603 young adult animals by Stimulated Raman Scattering (SRS). Representative images of a
 604 single focal plane of the first and second intestinal segments are shown. The anterior end of
 605 the worm is toward the left. For simplicity, *daf-22(ok693)* will be referred to as *daf-22(-)*
 606 thereafter. (B) As in (A), but with representative images of entire larval stage L4 worms at a
 607 focal plane with the strongest SRS intensity. (C) Quantification of LD diameter of WT,

608 *tmem-120(hj50)*, *daf-22(-)* and *daf-22(-); tmem-120(hj50)* larval L4 stage worms (n = 10 for
609 each strain), using DHS-3::mRuby (*hj200*) as a LD marker. Each data point represents the
610 average LD diameter of an individual worm. Total number of LDs quantified: WT = 2033,
611 *tmem-120(hj50)* = 1561, *daf-22(-)* = 1331 and *tmem-120(hj50); daf-22(-)* = 1337. (D) Label
612 free quantification of neutral lipid content by SRS in WT (n=20), *tmem-120(hj50)* (n=20),
613 *daf-22(-)* (n=19) and *daf-22(-); tmem-120(hj50)* (n=20) worm shown in (B). Each data point
614 represents neutral lipid content of an individual worm. The mean value of WT worms is
615 assigned as 1. a.u. = arbitrary unit. (E) Quantification of TAG level in WT and *tmem-*
616 *120(hj50)* L4 stage animals by LC-MS. Three independent biological samples for each group.
617 Each group consists of ~2000 worms. The mean value of WT worms is assigned as 1. (F)
618 Visualization of LDs in L4 stage worms using DHS-3::mRuby (*hj200*) as a LD marker.
619 Representative images of *daf-22(-)*, *daf-22(-); tmem-120(hj50)*, *daf-22(-); tmem-120(hj50);*
620 *Ex[vha-6p::tmem-120::sl2::gfp]* and *daf-22(-); tmem-120(hj50); Ex[vha-6p::mouse*
621 *tmem120A::sl2::gfp]* are shown. The GFP is expressed from the same operon as TMEM-120
622 or mouse TMEM120A, but not as a fusion protein. Each representative image is a projection
623 of 7.5 μ m z stack with the second intestinal segment in the center area. Enlarged LDs are
624 indicated by white arrowheads. For all graphs, bars or horizontal lines represent mean \pm SD.
625 Statistical analysis: (C-D) two-way ANOVA followed by Sidak's multiple comparisons test;
626 (E) unpaired t test. ***p < 0.001; ****p < 0.0001.

627

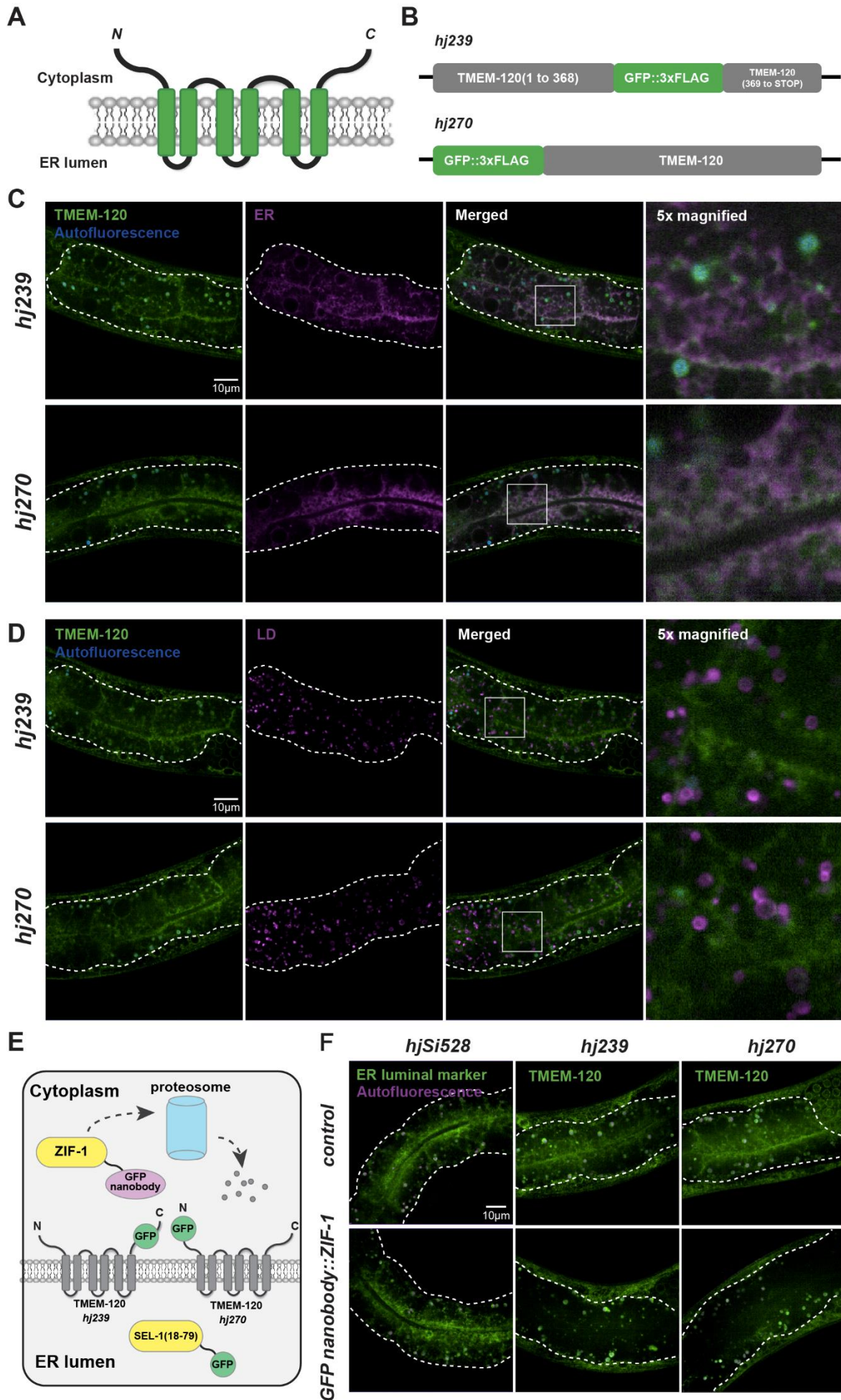


628

629 **Figure 2. TMEM-120 promotes the incorporation of fatty acids into TAG.** (A-B) The
 630 experimental design for monitoring deuterated oleic acid-d₃₄ (OA-d₃₄) uptake (A) or turnover
 631 (B). (C-D) Visualization of OA-d₃₄ incorporation (C) or turnover (D) by SRS in wild type
 632 (wt) and *tmem-120(hj50)* worms. Representative images of a layer with the strongest SRS
 633 signal in the first and second intestinal segments are shown. (E) Quantification of OA-d₃₄

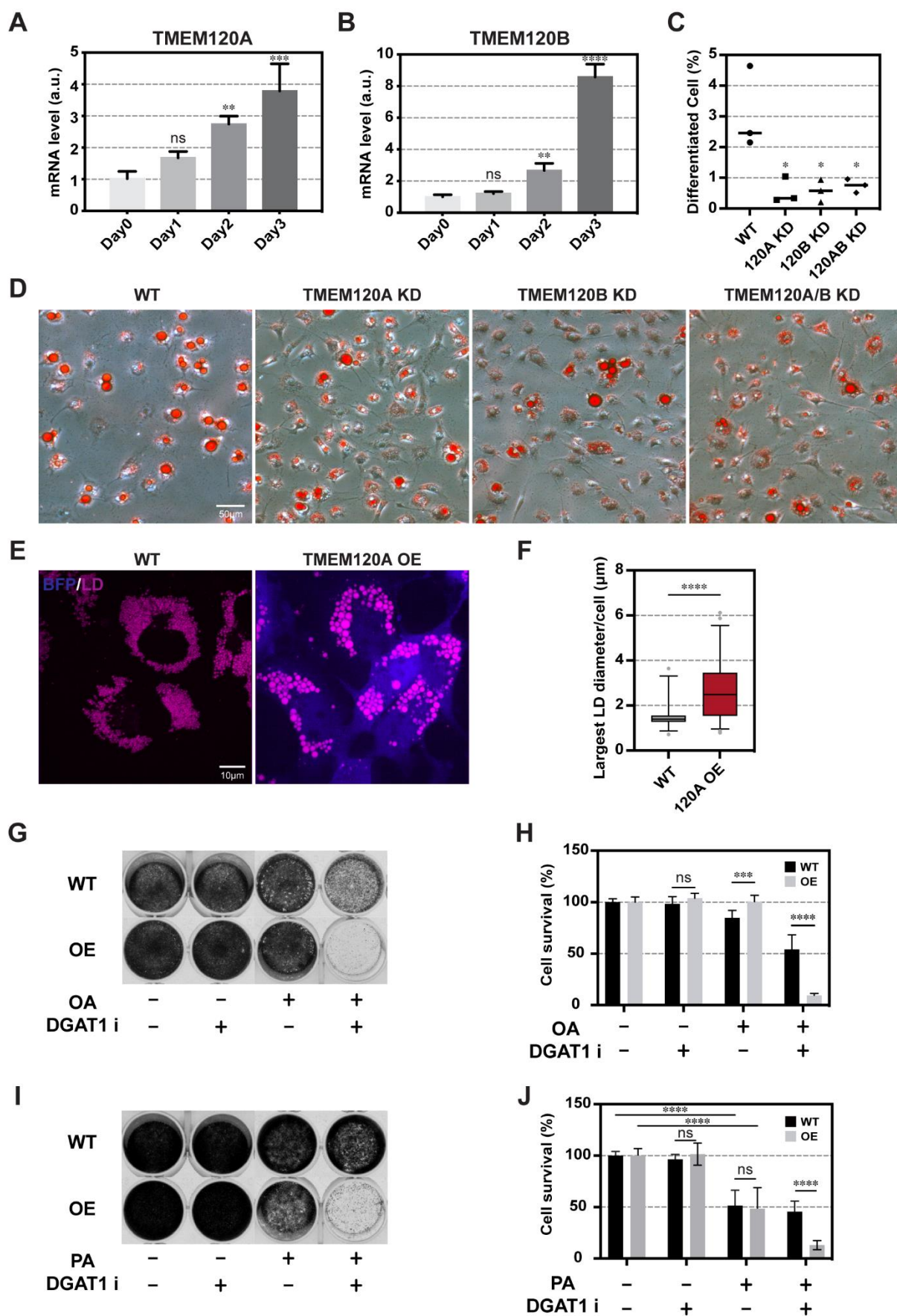
634 uptake in WT and *tmem-120(hj50)* worms shown in (C). n = 5 to 9 for each group at each
635 time point. Straight dashed lines and equations were generated based on linear regression
636 analysis of each group. (F) Quantification of OA-d₃₄ turnover in WT and *tmem-120(hj50)*
637 worms shown in (D). n = 7 to 10 for each group at each time point. Statistical analysis:
638 unpaired t test (for each time point). ns, not significant; ***p < 0.001.

639



641 **Figure 3. TMEM-120 is an ER resident protein.** (A) The topology of TMEM-120 based on
642 its homology with TMEM120A. (B) Schematic representation of TMEM-120 GFP fusion
643 proteins. (C) Visualization of TMEM-120 GFP fusion proteins and an intestinal-specific
644 luminal ER marker SEL-1(18-79)::mCherry::HDEL (*hjSi158*) in L4 worms. Representative
645 images of a single focal plane of the first and second intestinal segment are shown. For each
646 image, the intestine is enclosed by dashed lines. The boxed region in the merged image is 5x
647 magnified and shown as a separate panel. (D) As in (C), but with an LD marker DHS-
648 3::mRuby (*hj200*). (E) Schematic diagram on the GFP nanobody::ZIF-1 mediated
649 degradation of cytoplasmic GFP fusion proteins. GFP targeted to the ER lumen is protected
650 from degradation. (F) Visualization of an intestinal-specific luminal ER marker SEL-1(18-
651 79)::GFP::HDEL (*hjSi528*) and TMEM-120 GFP fusion proteins in L4 worms in the absence
652 (control) or presence of GFP nanobody::ZIF-1 (*hjSi524*). Each representative image is a
653 projection of 5 μ m z stack with the second intestinal segment in the center. The intestine is
654 enclosed by dashed lines. GFP signals in the hypodermis (regions outside the dashed lines)
655 were unaffected by GFP nanobody::ZIF-1.

656



658 **Figure 4. TMEM120A promotes adipogenesis and LD expansion in mammalian cells.**

659 (A-B) The expression level of TMEM120A and TMEM120B during OP9 pre-adipocyte
660 differentiation measured by real time PCR. Mean + SD from three independent samples is
661 shown. (C) Quantification of mature OP9 adipocytes (at least one LD >15 μ m / cell). Data
662 summarized from three independent experiments. Each data point represents the percentage
663 of mature adipocytes in one experiment. Total number of cells analyzed: WT, 4988 cells;
664 TMEM120A KD, 5216 cells; TMEM120B KD, 6107 cells; TMEM120A+TMEM120B KD:
665 3898 cells. Horizontal line represents the mean. (D) Visualization of LDs in differentiated
666 WT, TMEM120A KD, TMEM120B KD, and TMEM120A/B KD OP9 cells by Oil Red O
667 staining. (E) Visualization of LDs in oleic acid treated wild type (WT) and TMEM120A
668 overexpressing (OE) COS7 cells with FAS lipid droplet dye. Three independent experiments
669 were performed. Each representative image is a projection of 5.5 μ m (WT) or 6.5 μ m (OE) z
670 stack. (F) Quantification of the largest LD diameter of oleic acid treated WT and
671 TMEM120A OE COS7 cells. Three independent experiments were performed. Total number
672 of cells analyzed: WT: 183 cells. OE: 239 cells. (G) Assessment of cell survival by crystal
673 violet staining after 20 hours of oleic acid (OA) and DGAT1 inhibitor (DGAT1i, A922500)
674 treatment. Solvent control: ethanol (oleic acid) and DMSO (DGAT1i). (H) Quantification of
675 cell survival, based on extracted crystal violet from (G). Data summarized from 9
676 independent wells, performed on 3 separate days, for each cell line. Mean + SD is shown. (I)
677 As in (G), but with palmitic acid (PA). (J), As in (H), but with cells treated with palmitic acid
678 (PA). Statistical analysis: (A-B) One-way ANOVA followed by Dunnett's multiple
679 comparisons test; (C and F) unpaired t test; (H-J) multiple t-test. ns, not significant; *p<0.05;
680 **p<0.01; ***p<0.001; ****p<0.0001.

A

```

C. elegans 1 - - - - -MATEKLDSEWKLVQDDFQKLEKIHDEYIQKSRQVSKFQETAGKAMKHNNYLKLNKE TMRQAQSSAEKLD EADTSKTDVLSHVAKLREEL 90
Mouse 1 MQSPPPDPLGDCLRNWEDLQDDFQGIQETHRLYRLKLEELTKLQANCTNSITRQKRLQELALVLKCKRPSL - - - - -P - - - - -SESMEAAQEL ENQM 87
Human 1 MQPPPPGPLGDCLRDWEDLQDDFQNIQETHRLYRLKLEELTKLQNNCTSSITRQKRLQELALALKCKKPSL - - - - -P - - - - -AEAEAAQEL ENQM 87

C. elegans 91 AVANLRIRDMQGE LPAQTNGFYLNLI LGSNLNVSLLTKAEKFKYKQEYEGFKWSITILIC-LLALCAWIWFRVFDLSLCFLMVWYCTLTIRESV 185
Mouse 88 KERQGLFFDMEAYL - PKKNGLYLSLVLG - NVNVTL LSKQAKFAYKDEYEFKLYLTIILIVISFTQRFLNLSRVTDAAFNFLVWYCTLTIRESI 181
Human 88 KERQGLFFDMEAYL - PKKNGLYLSLVLG - NVNVTL LSKQAKFAYKDEYEFKLYLTIILILISFTQRFLNLSRVTDAAFNFLVWYCTLTIRESI 181

          hj49(G195E)

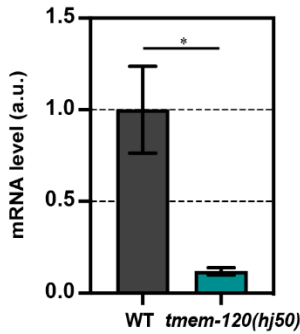
C. elegans 186 LRVNGSKIKGWWLSHHYLSCAVPGIVLTWKDGLCYQEFRPYFLIFTFYISLVQLAQNYQSGCLRRHS LGQGHQMDITVEGFTSWQFKGLTFLLP 281
Mouse 182 LIINNGSRIKGWWVFHHYVSTFLSGVMLTWPDGLMYQKFRNQFLSFSMYQSFVQFLQYYYQSGCLYLRALGERHTMDLTVEGFQSWMWRGLTFLLP 277
Human 182 LIINNGSRIKGWWVFHHYVSTFLSGVMLTWPDGLMYQKFRNQFLSFSMYQSFVQFLQYYYQSGCLYLRALGERHTMDLTVEGFQSWMWRGLTFLLP 277

          hj50(Q290*)

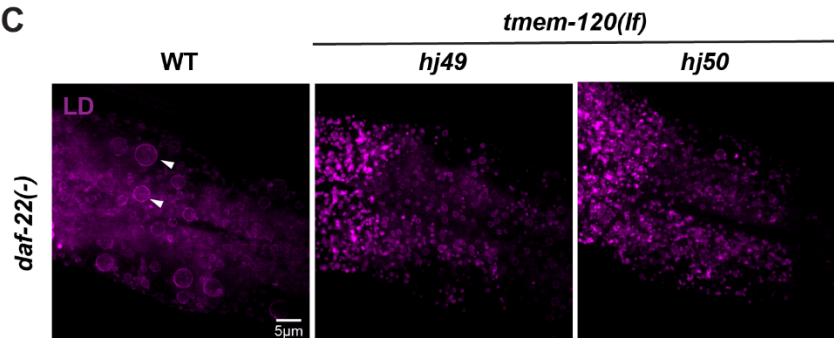
C. elegans 282 FLA FGYLYQLYLAWK LFGYTNS ETC DGI MQVWTL SLL LGL IAGNIVIT TSMVCIRKFKTSTSYTNIVTLTRKYSSRRNIREAPPTPELLRGAPPPP 377
Mouse 278 FLFFGHFWQLFNALTLFNLRADPECKE - WQVLMCGFPFLLLFLGNFFTL LRVVHQK FHSQGHGNKKD - - - - - 343
Human 278 FLFFGHFWQLFNALTLFNLRADPQCKE - WQVLMCGFPFLLLFLGNFFTL LRVVHHK FHSQRHGSKKD - - - - - 343

C. elegans 378 TGKHLHLH
Mouse
Human
    
```

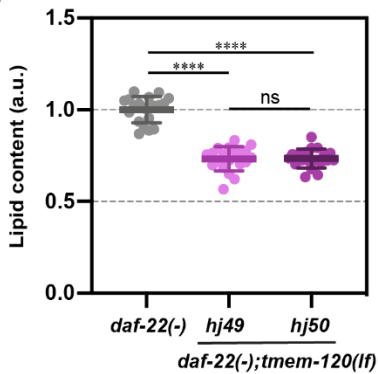
B



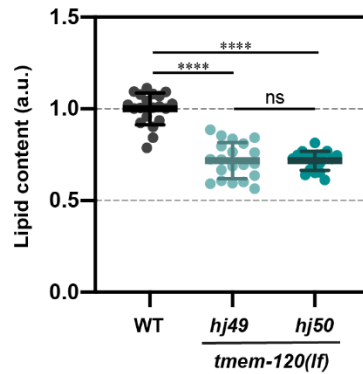
C



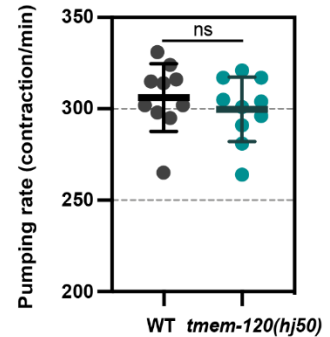
D



E



F

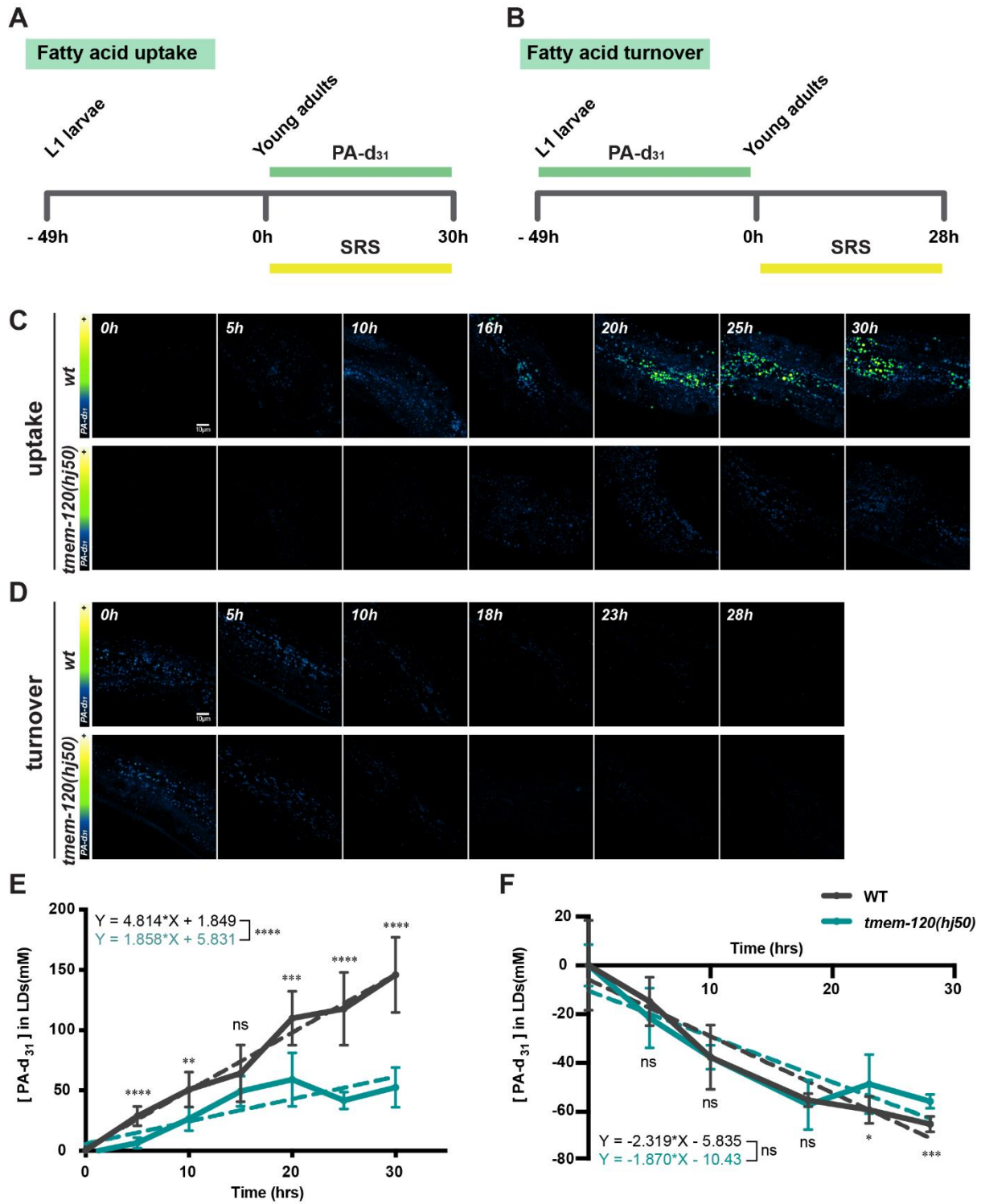


681

682 **Figure S1. TMEM-120 promotes LD expansion.** (A) Sequence alignment of *C. elegans*
 683 TMEM-120, mouse TMEM120A and human TMEM120A. Identical residues are shaded in
 684 grey. The mutated residues encoded by *tmem-120(hj49)* and *tmem-120(hj50)* are labeled red.
 685 (B) Expression level of *tmem-120* in wild type (WT) and *tmem-120(hj50)* L4 stage worms
 686 measured by real time PCR. Two independent samples for each strain. The mean value of
 687 WT is set as 1 for comparison. (C) Visualization of LDs in *daf-22(-)*, *daf-22(-); tmem-*
 688 *120(hj49)* and *daf-22(-); tmem-120(hj50)* larval L4 stage worms using DHS-3::mRuby
 689 (*hj200*) as a LD marker. Each representative image is a projection of 7.5µm z stack with the
 690 second intestinal segment in the center. Enlarged LDs are indicated by white arrowheads. (D)

691 Label free quantification of neutral lipid content in *daf-22(-)* (n=20), *daf-22(-); tmem-*
692 *120(hj49)* (n=20) and *daf-22(-); tmem-120(hj50)* (n=19) L4 stage worms by SRS. Each data
693 point represents the neutral lipid content of an individual worm. (E) As in (D), but with WT
694 (n=20), *tmem-120(hj49)* (n=20) and *tmem-120(hj50)* (n=19) L4 stage worms. (F) Pharyngeal
695 pumping rate of WT (n=10) and *tmem-120(hj50)* (n=10) 1-day old adult worms. Each data
696 point represents the contraction rate of an individual worm. For all graphs, bars or horizontal
697 lines represent mean \pm SD. Statistical analysis: (B and F) unpaired t test; (D and E) one-way
698 ANOVA followed by Tukey's multiple comparisons test. a.u., arbitrary unit. ns, not
699 significant; * $p < 0.05$; **** $p < 0.0001$.

700

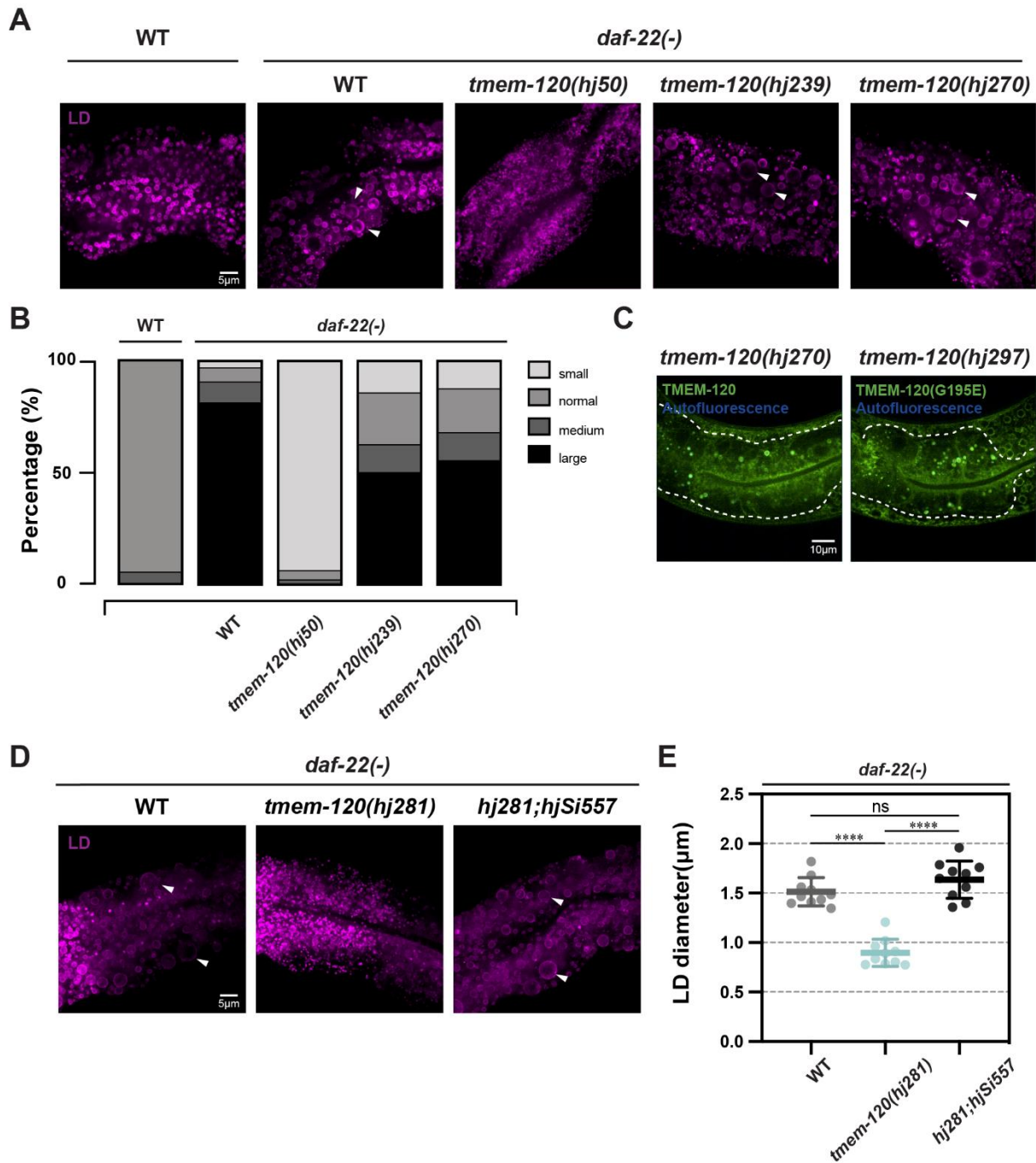


701

702 **Figure S2. TMEM-120 promotes the incorporation of fatty acids into TAG.** (A-B) The
 703 experimental design for monitoring deuterated palmitic acid-d₃₁ (PA-d₃₁) uptake (A) or
 704 turnover (B). (C-D) Visualization of PA-d₃₁ incorporation (C) or turnover (D) by SRS in wild
 705 type (wt) and *tmem-120(hj50)* worms. Representative images of a layer with the strongest
 706 SRS signal in the first and second intestinal segments are shown. (E) Quantification of PA-

707 d_{31} uptake in WT and *tmem-120(hj50)* worms shown in (C). n = 5 to 9 for each group at each
708 time point. Straight dashed lines and equations were generated based on linear regression
709 analysis of each group. (F) Quantification of PA- d_{31} turnover in WT and *tmem-120(hj50)*
710 worms shown in (D). n = 4 to 9 for each group at each time point. Statistical analysis:
711 unpaired t test (for each time point). ns, not significant; *p < 0.05; **p < 0.01; ***p <
712 0.001; ****p < 0.0001.

713



714

715 **Figure S3. Functional characterization of TMEM-120 GFP fusion proteins. (A)**

716 Visualization of LDs in wild type (WT), *daf-22(-)*, *daf-22(-); tmem-120(hj50)*, *daf-22(-);*

717 *tmem-120(hj239)* and *daf-22(-); tmem-120(hj270)* L4 stage worms, using DHS-3::mRuby

718 (*hj200*) as a LD marker. Each representative image is a projection of 7.5µm z stack with the

719 second intestinal segment in the center. Enlarged LDs are indicated by white arrowheads. (B)

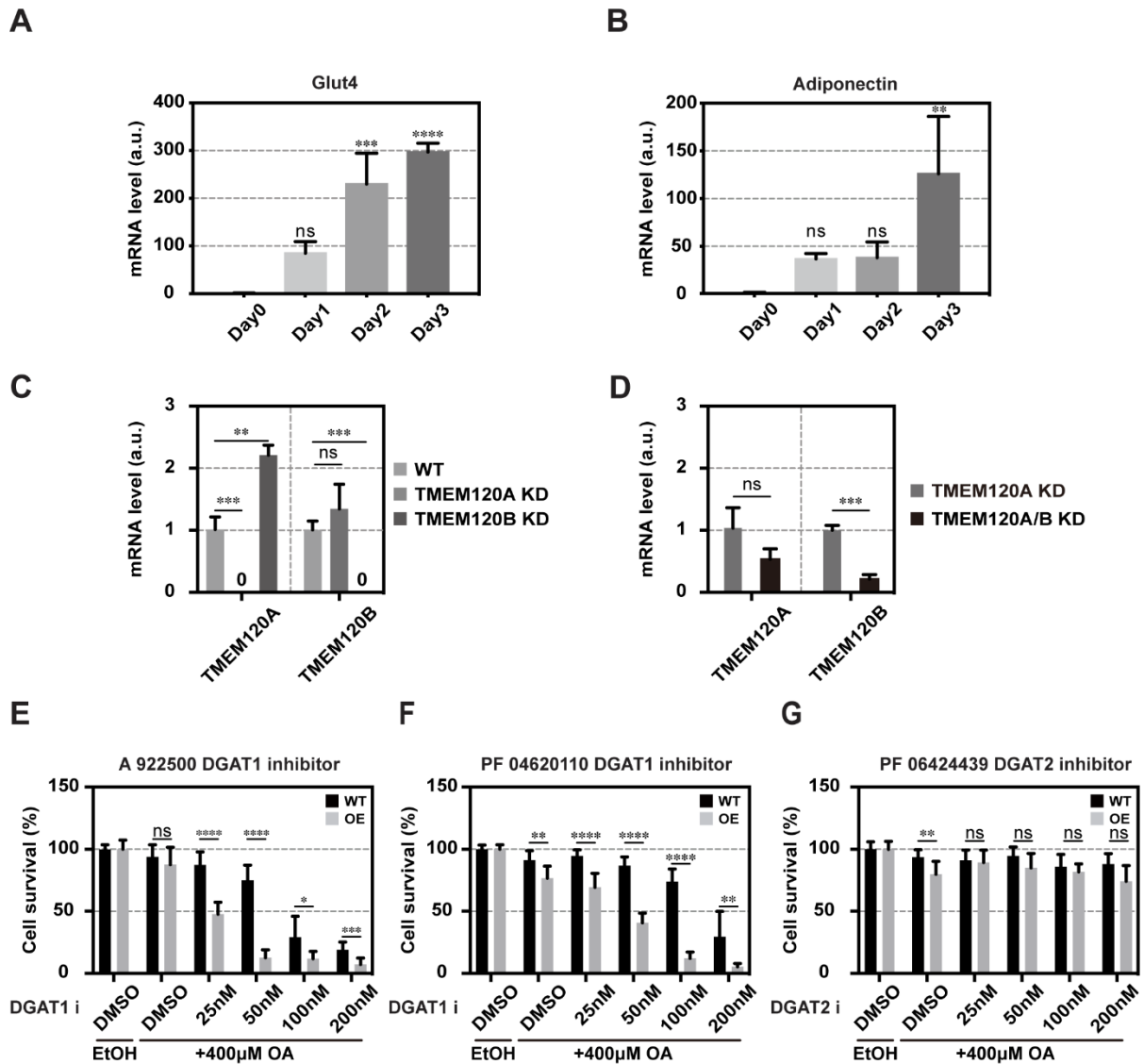
720 Quantification of percentage of WT (n=57), *daf-22(-)* (n=64), *daf-22(-); tmem-120(hj50)*

721 (n=48), *daf-22(-); tmem-120(hj239)* (n=56) and *daf-22(-); tmem-120(hj270)* (n=56) 5-day old

722 adult worms with small ($D_L < 1.0\mu\text{m}$), normal ($1.0\mu\text{m} < D_L < 3\mu\text{m}$), medium ($3\mu\text{m} < D_L <$

723 5 μ m) and large (5 μ m < D_L) LDs. D_L, diameter of the largest LD in the second intestinal
724 segment of an individual worm. Data combined from 3 independent groups of worms (n = 14
725 to 22 for each group) for each strain. (C) Visualization of GFP::*TMEM-120* (*hj270*) and
726 GFP::*TMEM-120*(G195E) (*hj297*) in L4 stage worms. Representative images of a single
727 focal plane of the first and second intestinal segments are shown. The intestine is enclosed by
728 dashed lines. (D) Visualization of LDs in *daf-22(-)* and *daf-22(-); tmem-120(hj281)* and *daf-*
729 *22(-); tmem-120(hj281); hjSi557[vha-6p::*gfp>::tmem-120]* L4 stage worms, using DHS-
730 3::*mRuby* (*hj200*) as a LD marker. *tmem-120(hj281)* was generated by Cre-loxP based
731 excision of *tmem-120(hj239)*. Each representative image is a projection of 7.5 μ m z stack with
732 the second intestinal segment in the center. Enlarged LDs are indicated by white arrowheads.
733 (E) Quantification of LD size of worms from (D). Each data point represents average LD
734 diameter of an individual worm. Total number of LDs quantified: *daf-22(-)* = 1276, *daf-22(-);*
735 *tmem-120(hj281)* = 1216 and *daf-22(-); tmem-120(hj281); hjSi557* = 1279. Horizontal bars
736 represent mean \pm SD. Statistical analysis: one-way ANOVA followed by Tukey's multiple
737 comparisons test. ns, not significant; ****p < 0.0001.*

738



739

740 **Figure S4. TMEM120A acts upstream of DGAT1 in mammalian cells.** (A-B) The
 741 expression level of mature adipocyte markers Glut4 and Adiponectin during OP9 pre-
 742 adipocyte differentiation measured by real time PCR. Mean + SD from three independent
 743 samples is shown. The mean value on Day 0 is set as 1. a.u., arbitrary unit. (C) The
 744 expression level of TMEM120A and TMEM120B in wild type (WT), TMEM120A KD,
 745 TMEM120B KD cells, measured by real time PCR. Mean + SD from three independent
 746 samples of each cell line is shown. The mean value of WT cells is set as 1. (D) The
 747 expression level of TMEM120A and TMEM120B in TMEM120A KD (parental to the double
 748 KD cells) and TMEM120A+TMEM120B KD cells, measured by real time PCR. Mean + SD
 749 from three independent samples of each cell line is shown. The mean value of TMEM120A
 750 KD cells is set as 1. (E) Quantification of cell survival for WT and TMEM120A
 751 overexpressing (OE) COS7 cells treated with oleic acid (OA) and increasing concentration of

752 DGAT1 inhibitor (A922500), based on crystal violet staining. Solvent control: ethanol (oleic
753 acid) and DMSO (DGAT1i). Data summarized from 9 independent wells, performed on 3
754 separate days, for each cell line. Mean + SD is shown. (F) As in (E), but with DGAT1
755 inhibitor (PF 04620110). (G) As in (E), but with DGAT2 inhibitor (PF06424439). Statistical
756 analysis: (A-B) One-way ANOVA followed by Dunnett's multiple comparisons test. (C-D)
757 unpaired t-test; (E-G) multiple t-test. ns, not significant; * $p < 0.05$; ** $p < 0.01$; *** $p < 0.001$;
758 **** $p < 0.0001$.